Multifaceted analysis of micro/nanoparticles in Hopedale's snow: comprehensive characterization, cellular assessments, and implications for environmental health

Maan, Zeina; Sakib, Sadman; Jakubek, Zygmunt J.; Zou, Shan; Tuglavina, Elizabeth; Pijogge, Liz; Liboiron, Max

https://doi.org/10.4224/dc66-q984

Multifaceted Analysis of Micro/Nanoparticles in Hopedale's Snow: Comprehensive Characterization, Cellular Assessments, and Implications for Environmental Health

Non-sensitive

Cite as “Multifaceted Analysis of Micro/Nanoparticles in Hopedale's Snow: Comprehensive Characterization, Cellular Assessments, and Implications for Environmental Health Chen, M.; Jakubek, Z. J.; Maan, Z.; Zou, S. Report No. NM-2025-0004, National Research Council of Canada, DOI:**10.4224/dc66-q984**.

Report No. NM-2025-0004
May 30, 2025
Note: **The Nunatsiavut Government owns sample data**.

Zeina Maan, Sadman Sakib, Zygmunt J. Jakubek, Shan Zou*
Metrology Research Center, National Research Council Canada, Ottawa, ON K1A 0R6, Canada
Elizabeth Tuglavina, Liz Pijogge
Nunatsiavut Government, Nain, NL A0P 1L0, Canada
Max Liboiron
Memorial University of Newfoundland and Labrador, St. John’s, NL A1B 1T5, Canada

*Corresponding author: Shan Zou (shan.zou@nrc-cnrc.gc.ca)

Abstract

This study presents an in-depth analysis of small particles in snow samples collected from six sites in Hopedale, Nunatsiavut, Newfoundland and Labrador, Canada. Eighteen samples (three per site) were processed to assess the presence, size, concentration, and potential cellular effects of particles. Samples were filtered and classified into two groups: Group A (particles <1 µm, mean size 100–200 nm) and Group B (particles >5 µm). Particle characterization was performed using dynamic light scattering and nanoparticle tracking analysis. Cellular assays were conducted to evaluate potential biological impacts. Results showed that particle size was consistent across locations while particle concentrations varied. The presence of larger particles suggested aggregation or sedimentation of smaller ones. These larger particles showed minimal cellular effects, likely due to their low concentrations. No consistent correlation was observed between particle number and cell viability. The study enhances our understanding of particulate matter in snow and highlights the importance of considering the origin and composition of particles in toxicity assessments.

Graphical Abstract

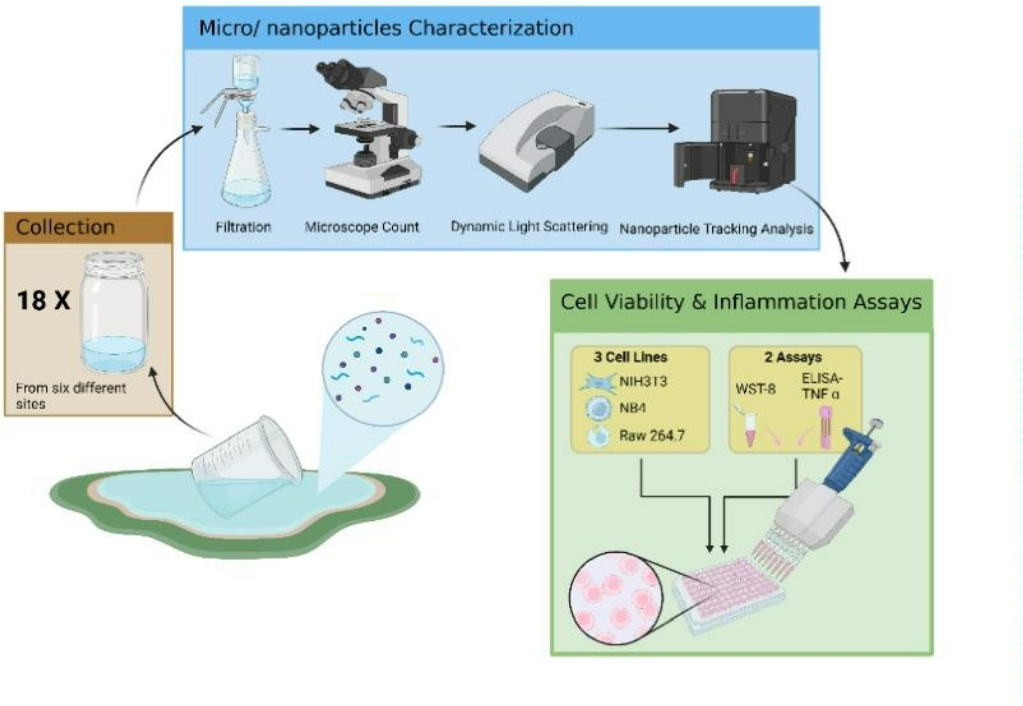

Keywords: micro/nanoparticles, environmental samples, comprehensive characterization, cellular assessments, nanoparticle tracking analysis (NTA), dynamic light scattering (DLS), snow, Nunatsiavut.

Introduction

The Arctic region plays a vital role in maintaining the overall health and dynamics of our planet's ecosystems. With the ongoing challenge of climate change, understanding and monitoring the environmental conditions in this ecosystem is of utmost importance.[1-2] Industrial activities, including pollution, large-scale fishing, and climate change, are significantly impacting Arctic marine ecosystems, posing threats to Indigenous communities and the region's global importance.[3-4] The intensification of industrial uses, driven by factors like increased accessibility, is altering Arctic ecosystems and compromising the delivery of vital ecosystem services, with pollution stemming from various sources, including settlements, tourism, shipping, and resource extraction, further exacerbating these challenges .[5-6] Previously, a comprehensive assessment of anthropogenic particles (APs), including microfibers and microplastics, was conducted in samples from across the Canadian Arctic between 2014 and 2017, onboard the Arctic research vessel CCGS Amundsen. The assessment revealed high concentrations of APs, primarily composed of microfibers. It suggests that the Arctic serves as a significant sink for these pollutants, highlighting the need for ongoing monitoring to assess temporal trends and evaluate the impact of mitigation measures and climate change.[7] Environmental snow, ice, or water samples contain diverse microplastics, such as fragments, fibres, and microbeads,[8-11] with sizes ranging from nanometers to millimetres.[12] In addition, microparticle pollutants, including heavy metals such as mercury and lead,[13-14] persistent organic pollutants,[15] black carbon from fossil fuel combustion,[16-17] and radioactive contaminants from nuclear activities, have been identified.[18]

Recent international efforts, including those led by the Arctic Council's Arctic Monitoring and Assessment Programme (AMAP), have underscored the importance of monitoring anthropogenic particles, such as microplastic pollution, in polar environments due to their potential ecological and human health impacts.[19-20] These particulates have been shown to interact with biological systems and elicit cellular responses, such as oxidative stress, inflammation, and cell death, depending on their size, surface chemistry, and composition.[21-22] In this context, cellular models can provide a valuable tool for evaluating the biological reactivity of environmental particles. While chemical and physical characterization remains essential, in vitro assessments of cell viability and inflammatory response offer direct insight into the potential health relevance of real-world particulate exposures. Such

approaches are particularly pertinent in the Arctic, where vulnerable ecosystems and subsistence communities may be disproportionately affected by the accumulation of contaminants. Therefore, this study aims to bridge particle characterization with biological assessment by evaluating the cellular impacts of snow-derived particles in multiple mammalian cell types, contributing to a more comprehensive understanding of their potential toxicity and environmental significance.

Here, we report on the significance and implications of micro- and nanoparticles in snow from Hopedale, Nunatsiavut. This study attempts to bridge the gap between particle characterization and biological response. Accordingly, we characterize the size and size distribution of micro- and nanoparticles in the snow samples using microscopic examination, dynamic light scattering (DLS), and nanoparticle tracking analysis (NTA) and assess their impact on cellular viability. Additionally, the investigation aims to explore the correlations between the number and size of nano- and microparticles from different sites and potential levels of inflammation. In this work, we define nano- and microparticles in a broad sense as those with characteristic dimensions, such as hydrodynamic diameter, smaller than 1 μm and larger than 1 nm, respectively.

Materials and Methods

Snow sample processing

Eighteen snow samples were collected from the Hopedale region at six randomly selected sites by a Nunatsiavut beneficiary familiar with the area. Locations include Dump Pond (DP), Ellen Island (EI), Base Hopedale (B), Berry Road (BR), Black Heads (BH), and Trout Ponds (TP). Three bottles (with approximately 500 mL each) of snow samples were collected from each site (melted to water upon receipt). Samples were autoclaved and then subjected to vacuum filtration as the first step, where they were divided into two main groups: Group A, consisting of filtrates, was obtained after filtering with a 1 μm PTFE filter, and Group B, comprising particles, was collected from a 5 μm stainless steel mesh filter. It is important to note that the particles in *Group B* (larger than 5 μm) were left unsuspended, whereas particles in *Group A* (smaller than 1 μm) largely remained dispersed in water. In all the experiments detailed within this report, the three bottles received from each site were randomly numbered and used sequentially,

following an order where the second bottle was not employed until the completion of the first, and so on. Both *Groups A* and *B* underwent distinct phases of analysis, i.e., concentration assessment, size assessment, and cellular response evaluation, as shown in Figure 1.

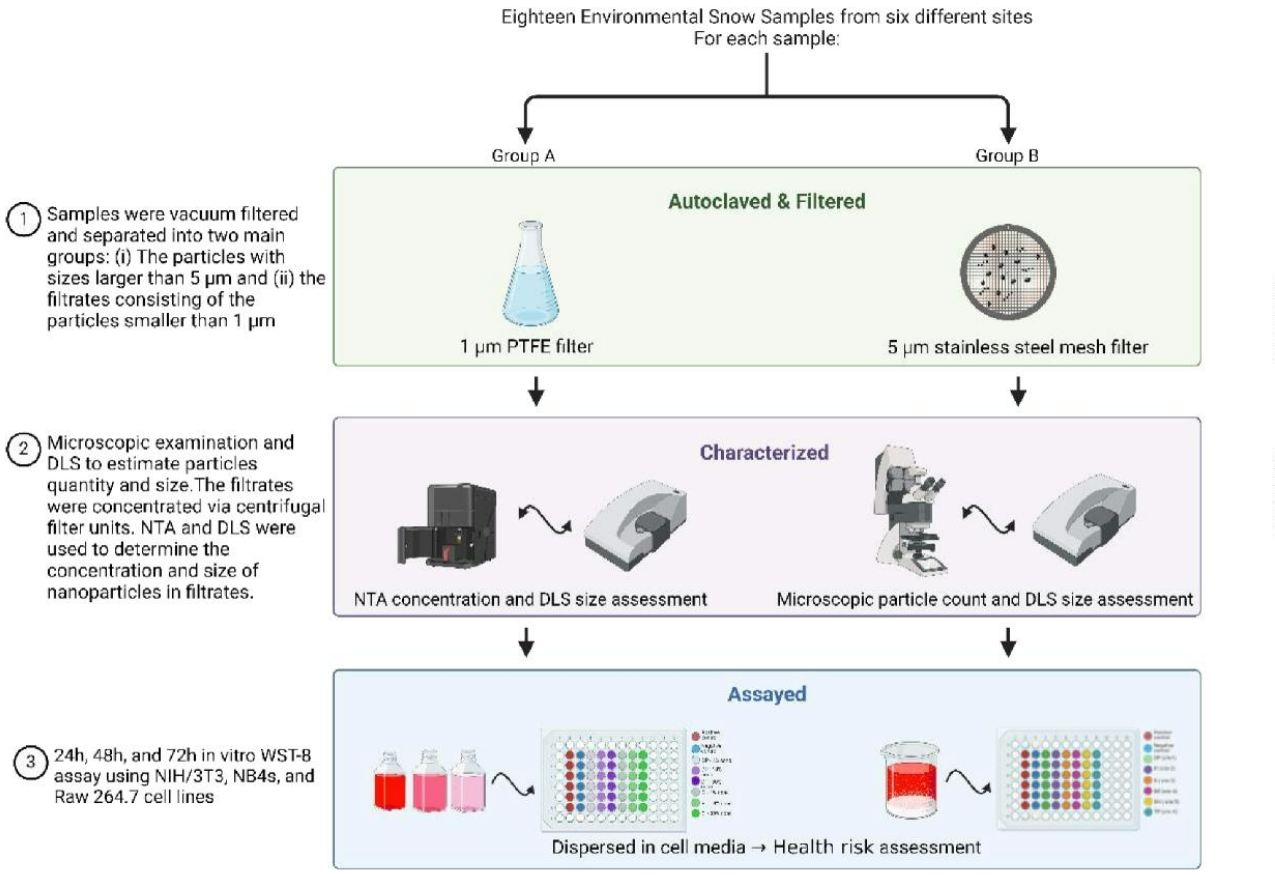

Figure 1. Schematic illustration of each of the six-sample processing workflow for 150 mL per sample.

Reagents

Cell media such as Dulbecco's modified Eagle's medium (DMEM) and F-12K, fetal bovine serum (FBS), penicillin-streptomycin, and mouse enzyme-linked Assay (ELISA) kit of tumour necrosis factor-alpha (TNF-α) were purchased from Gibco (Thermo Fisher Scientific Inc., Canada). NIH3T3 (mouse embryonic fibroblasts, normal cells), NB4 (acute myelocytic leukemia cancer cells), and Raw 264.7 (male mouse-induced monocyte/macrophage-like cells) were purchased from American Type Culture Collection (ATCC, USA). Cell viability studies were performed in 96-well, flat-bottom plates (BD Falcon, purchased

from VWR International LLC., Canada), using a WST-8 Cell Counting Kit 8 (2-(2-methoxy-4-nitrophenyl)-3-(4-nitrophenyl)-5-(2,4-disulfophenyl)-2H-tetrazolium monosodium salt) (purchased from Cedarlane, Canada).

Concentration of group A samples

To concentrate the filtrates for DLS measurements and further for cell viability assessments, centrifugal filter units (Amicon® Ultra, 30 kDa MWCO, MilliporeSigma, USA) were used in a two-step concentration process: five 10 mL aliquots were first concentrated to 1 mL each, then pooled and further reduced to 500 µL within 10 minutes at 4400 rpm. However, some membrane fouling occurred, likely due to the use of centrifugal force to drive filtration rather than repeated recirculation through membranes and tubing.[23] This method achieved a 100-fold concentration of the diluted, polydisperse samples with minimal loss or contamination.

Characterization of group A samples by dynamic light scattering and nanoparticle tracking analysis

Dynamic light scattering and nanoparticle tracking analysis are commonly used techniques for assessing the size of submicron particles and, to a varying extent, particle concentration. Both methods work satisfactorily well for monomodal and monodisperse (or nearly monodisperse) samples but show limitations with more complex ones, such as polydisperse samples of environmental origin. Combining both techniques can overcome some of the limitations.

DLS measures fluctuations in scattered light intensity caused by the Brownian motion of particles, yielding an intensity autocorrelation function, which provides information about the diffusion of particles and, in turn, their size distribution via the Stokes-Einstein equation.[24] Total scattered light intensity expressed as a derived count rate (DCR) is proportional to particle concentration. Still, the relationship is nontrivial, as the proportionality factor depends on size, refractive index, and other properties of light-scattering particles. In this study, measurements were conducted using Zetasizer Nano ZS (Malvern Panalytical, UK) at a fixed position (4.65 mm) and full laser power (attenuation level 11). Samples of autoclaved dispersions in disposable polystyrene semi-micro cuvettes (VWR, cat# 97000-586) were equilibrated in a sample compartment for 300 s before the measurements were

conducted at 25 °C. Three indications were recorded for each measurement, each consisting of a minimum of ten 10-s-long runs. Data analyses were performed using Zetasizer Software (versions 7.13 and 8.0 Pro) with the default water viscosity and refractive index values of 0.8872 mPa·s and 1.330, respectively, and an assumed material refractive index value of 1.59 equal to that of polystyrene. Preliminary analyses revealed that the obtained samples were too dilute to conduct DLS measurements, as even at the maximum laser power, the mean scattered photon count rates were significantly below the manufacturer's recommended minimum value of 150 kcps (kilocounts of photons per second). Consequently, all samples were concentrated 16-fold for the final measurements. The DLS analysis results are reported as the average intensity-weighted particle size distribution calculated for each site from three indications, with the particle size defined as a sphere-equivalent hydrodynamic diameter. For monomodal and (nearly)monodisperse samples, cumulants analysis is usually conducted, and results are reported as a sphere-equivalent intensity-weighted harmonic average (Z-average, Z-avr) hydrodynamic diameter and polydispersity index (PdI). However, neither of the six samples satisfied the monodispersity requirement; consequently, the cumulants analysis was not applicable.

NTA follows the Brownian motion of light-scattering particles using a camera.[25-26] Tracks of individual particles are recorded and analyzed to determine particle diffusion rates and particle sizes via the Stokes-Einstein relationship. By tracking and counting multiple particles simultaneously, sample size distribution and particle concentration are determined.[26] The reported measurements were conducted using NanoSight LM10-HS (Malvern Panalytical, UK) with the instrument operated and data analyzed using NanoSight NTA 3.0 software. The instrument covers a nominal particle size range from 10 nm to 1 µm, with the lower size limit strongly depending on the physical nature and properties of the investigated particles. It is usually somewhat higher in the (10 to 50) nm range for complex, polydisperse samples.[27] Since NTA simultaneously tracks multiple individual particles, size distribution and concentration measurements are typically conducted with particle concentrations lower by two to three orders of magnitude than those required for DLS.[28] The manufacturer recommended sample concentration in the (10^7 to 10^9) particles/mL range, which correlates with (20 to 100) particles/frame. Accordingly, the Group A samples were analyzed as obtained.

Each measurement consisted of five 60-s-long video acquisitions at an optimized camera level of 11, with new aliquots advanced manually between acquisitions. Sample temperature was measured for each of the five runs and recorded manually. During the analysis, the detection threshold was adjusted so that all recognizable particles were successfully identified. Auto settings for blur, maximum jump distance, and minimum track length were used. Water viscosity was set by NanoSight NTA 3.0 according to the measured temperature. Results are reported as the average particle size distribution and number concentration calculated from five acquisitions for each site.

Microscopic count for concentration assessment of Group B samples

The collected particles of Group B on filters were visually examined, and images were captured using an optical microscope (Echo Revolve RVL-100, Echo Laboratories, USA) with a 10× objective in bright field imaging mode. Particles from six images per site were counted, and calculations were performed to approximate the number of particles per filter, considering the actual areas of view and filter size. This value was then used to derive a rough estimate of particle concentration per site.

Cell culture

NIH3T3, NB4, and RAW 264.7 cells were cultured in DMEM supplemented with 10% fetal bovine serum (FBS) at 37°C in a humidified atmosphere containing 5% CO_2, with media changes every 48 hours. This culture medium was chosen for its compatibility with all three mammalian cell lines, providing essential nutrients and a stable environment to assess particle-induced effects on cell viability and inflammatory responses.

WST-8 assay for assessment of cell viability

Cell viability assays evaluate the cytotoxic potential of substances by measuring their ability to inhibit cell growth or induce cell death via necrosis or apoptosis, ensuring materials do not pose significant risks to human health.[29] In this study, the WST-8 assay was used to assess cell viability. This assay is based on the enzymatic reduction of the tetrazolium salt WST-8 to a water-soluble formazan dye by

mitochondrial dehydrogenases in viable cells. The amount of formazan produced is directly proportional to the number of metabolically active cells, resulting in higher absorbance at 450 nm.[30]

Concentrated Group A samples were re-dispersed in DMEM supplemented with 10% FBS for testing at various concentrations. Two sets of comparisons were performed:

- **Set 1:** 0.1×, 1×, and 3× concentrations of Group A samples, tested on NIH3T3 and NB4 cells.
- **Set 2:** 0.1×, 1×, and 5× concentrations of Group A samples, tested on NIH3T3, NB4, and RAW 264.7 cells.

NIH3T3 fibroblasts, derived from mouse embryos, were used as representative healthy adherent cells. NB4 cells, a human suspension cell line from acute promyelocytic leukemia, were selected to model a cancerous cell response. RAW 264.7 cells, a semi-adherent macrophage cell line from a mouse tumor, were included in Set 2 due to their phagocytic nature and potential for particle uptake.

In both sets, cells were seeded at 10,000 cells/well in 96-well plates with 100 µL of media containing Group A samples. For Set 1, viability was assessed at 24 and 48 h post-treatment. For Set 2, absorbance was measured at a single 72 h time point. In all cases, 10 µL of WST-8 reagent was added per well and incubated for 2 h at 37 °C before measuring absorbance at 450 nm. Milli-Q water served as the vehicle control.

Table 1. Average count of particles ≥ 5 µm per 500 mL.

Site	in Group B samples	Estimated # of particles per well
DP	12780	102
B	17040	136
EI	17040	136
BR	154780	1238
BH	8520	68
TP	8520	68

NIH3T3 and NB4 cells were seeded at 10,000 cells/well in 96-well plates. Group B particles from each site were directly dispersed in 4 mL of complete DMEM, and 100 µL of the treated media was added to

each well at the concentrations listed in Table 1. WST-8 assays were conducted at 24, 48, and 72 h post-treatment using the same protocol described above.

All WST-8 viability assays were conducted with appropriate quality controls. Each treatment condition was performed in biological triplicates with technical triplicates. Media-only blanks (without cells or particles), treatment blanks (media with particles but without cells), and untreated cell controls were included on every plate to account for background absorbance and to establish baseline viability. All pipetting steps were performed using sterile, low-retention tips to minimize variability and prevent particle loss. Absorbance at 450 nm was normalized against the corresponding blank wells, and inter-assay consistency was ensured by repeating key treatment conditions across independent experiments.

ELISA assay for assessment of inflammation levels

Inflammation assays measure the immune response by assessing the release of inflammatory mediators, aiding studies on inflammatory diseases and the efficacy of anti-inflammatory drugs. Unlike cell viability assays, inflammation assays, such as ELISA, evaluate biomarkers of inflammation in serum, plasma, and cell culture medium supernatants.[31] An ELISA kit was used to detect and quantify the inflammatory cytokine TNF-α, one of the most abundant biomarkers of inflammation.[32] Group A samples from Site B at 0.1, 1, and 5× concentrations were tested in Raw 264.7 cells. After 48 and 72 h of treatment, the cell culture media was collected and centrifuged at 2000 g to remove any cell debris. Approximately 100 µL the cell culture supernatant was used to perform the assay per the manufacturer's instructions.

Results and Analysis

Particle size distribution and concentration assessment of group A samples by DLS and NTA

Figure 2 shows the normalized intensity-weighted hydrodynamic diameter distributions, along with one standard error interval, determined for Group A samples from each of the six sites by averaging three individual DLS measurements. The distributions are rather broad, spanning, to a varying degree, nearly the entire size range from 10 nm to 1 µm. Since the sample concentrations barely exceeded the minimum threshold for DLS analysis, a large variation was observed between distributions from each of the three indications at each site, as evidenced by rather broad one-standard-error intervals.

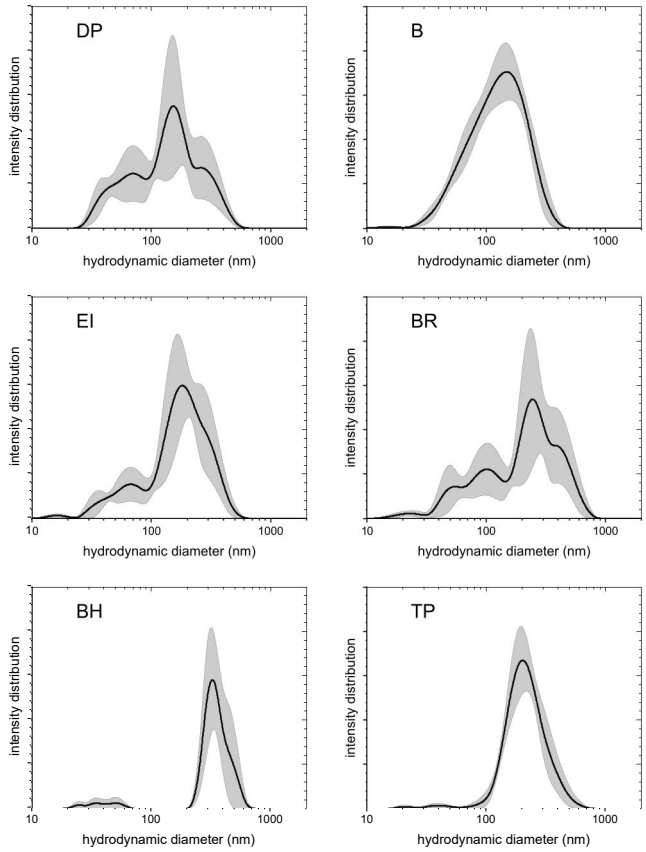

Figure 2. Normalized intensity-weighted hydrodynamic diameter distributions measured by dynamic light scattering. Solid lines and gray bands represent the average distribution, calculated from three indications, and the corresponding standard error interval, respectively.

Normalized number-weighted hydrodynamic diameter distributions determined by NTA are shown for each site in Figure 3, together with corresponding one standard error intervals. The number-weighted distributions appear to span (20 to 500) nm size range generally, thus narrower as compared to the intensity-weighted ones determined by DLS, with very few particles also observed between 500 nm and 1 μm, far too few to measure their statistically significant concentration.

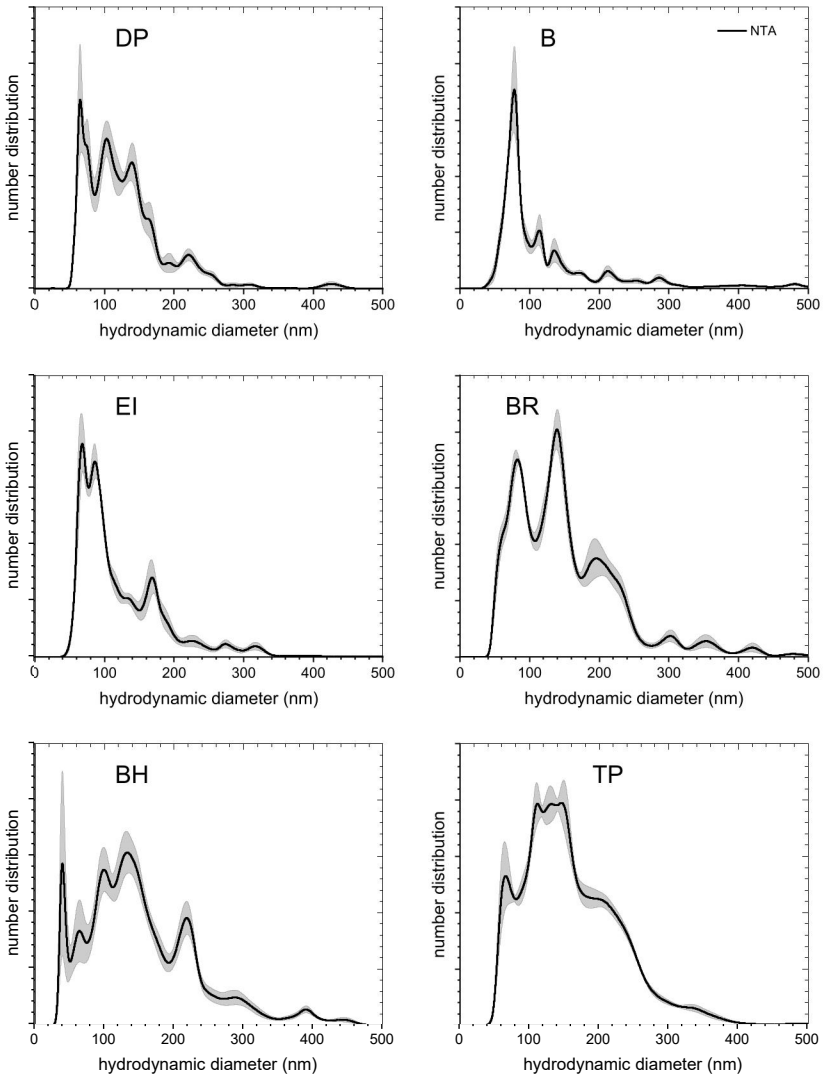

Figure 3. Normalized number-weighted hydrodynamic diameter distributions measured by nanoparticle tracking analysis. Solid lines and gray bands indicate the average distribution from five measurements, along with its corresponding standard error interval.

Quantitative comparison of the DLS and NTA native particle size distributions is shown in Tables 2-4, where d_I and d_N are intensity-weighted and number-weighted arithmetic average hydrodynamic diameters, respectively; S_I and S_N are spans of the distributions defined as (D90-D10)/D50 with D10, D50, and D90 being the hydrodynamic diameters corresponding to the 10^{th}, 50^{th}, and 90^{th} percentile of the respective distribution; DCR is the derived count rate; and C_N is the number concentration. DCRs represent scattered photon counts corrected for laser attenuation; therefore, monodispersed samples are proportional to particle number concentration.

Table 2: Summary of characterization of Group A samples by dynamic light scattering (DLS) and nanoparticle tracking analysis (NTA).

Site	DLS			NTA		
	d_I (nm)	S_I	DCR (kcps)	d_N (nm)	S_N	C_N (10^8 mL^{-1})
DP	158	1.83	143	130	1.11	5.1 (4)
B	138	1.42	205	137	2.15	9.2 (6)
EI	186	1.51	128	126	1.32	4.7 (5)
BR	238	1.77	241	154	1.33	15.4 (5)
BH	337	0.68	112	158	1.34	5.6 (3)
TP	225	1.01	673	164	1.17	25.1 (10)

Note: d_I is intensity-weighted arithmetic average hydrodynamic diameter from DLS measurements; d_N is number-weighted arithmetic average hydrodynamic diameter from NTA measurements; S_I and S_N are spans of the distributions defined as (D90-D10)/D50, where D10/D50/D90 are hydrodynamic diameter values corresponding to 10^{th}, 50^{th}, and 90^{th} percentiles of the respective distributions; DCR is derived count rate; and C_N is number concentration measured by NTA; see main text for explanation of site acronyms.

Table 3. Summary of particle size characterization of Group A samples by dynamic light scattering (DLS).

Site	**d_I (nm)**	**D_I10 (nm)**	**D_I50 (nm)**	**D_I90 (nm)**	**S_I**	**DCR (kcps)**
DP	158	49	140	305	1.8	143
B	138	57	127	237	1.4	205
EI	186	59	176	325	1.5	128
BR	238	60	223	454	1.8	241
BH	337	250	336	478	0.7	112
TP	225	134	209	345	1.0	673

Note: d_I is a sphere-equivalent intensity-weighted arithmetic average hydrodynamic diameter; D_I10, D_I50, and D_I90 are particle diameter values at 10^{th}, 50^{th}, and 90^{th} percentile of the particle size distribution; S_I is defined as (D_I90-D_I10)/D_I50 characterizes the relative width of the intensity-weighted particle size distribution; DCR is the derived count rate.

Table 4. Summary of particle size characterization of Group A samples by nanoparticle tracing analysis (NTA).

Site	d_N (nm)	D_N10 (nm)	D_N50 (nm)	D_N90 (nm)	S_N	C_N (10^8 mL^{-1})
DP	130	70	119	202	1.1	5.1 (4)
B	137	64	93	264	2.2	9.2 (6)
EI	126	67	100	199	1.3	4.7 (5)
BR	154	70	137	252	1.3	15.4 (5)
BH	158	76	137	259	1.3	5.6 (3)
TP	164	80	149	255	1.2	25.1 (10)

Note: d_N is a sphere-equivalent number-weighted arithmetic average hydrodynamic diameter; D_N10, D_N50, and D_N90 are particle diameter values at 10^{th}, 50^{th}, and 90^{th} percentile of the particle size distribution; S_N defined as $(D_N90-D_N10)/D_N50$ characterizes the relative width of the number-weighted particle size distribution; C_N is the number concentration; and the numbers in parentheses in the C_N column are one standard error in the units of the last digit of the concentration value.

The DLS- and NTA-determined size distributions, shown in Figures 2 and 3, respectively, appear significantly different for each site, and in fact, they are. The native DLS particle size distribution is intensity weighted as the total scattered light intensity is being measured; it emphasizes larger particles within a population since larger particles have, on average, a larger scattering cross section per particle. In NTA, light scattered by particles is also detected, but particles are counted individually, resulting in a number-weighted particle size distribution. However, not all particles are counted with the same efficiency. Due to the larger scattering cross section of larger particles, it is difficult to observe in a single laser instrument, such as used here, the smallest particles within a broad particle size distribution, short of running large acquisition sequences with samples diluted to a level of just a few particles per image frame (screen).

To facilitate a meaningful comparison of the reliability of the DLS- and NTA-determined distribution, both distributions were converted to volume-weighted ones. Conversion of a DLS-native intensity-weighted hydrodynamic diameter distribution to volume-weighted or number-weighted ones is not a trivial task as the per particle scattering cross section strongly varies with particle size and depends on particle refractive index and morphology. It is important to note that such conversions frequently lead to unreliable results and are generally strongly discouraged. Conversion of an NTA-native number-weighted distribution to a volume-weighted one, although a somewhat simpler process, may also lead

to unreliable results, particularly for oddly shaped particles with inhomogeneous morphology. Since the nature and properties of the particles analyzed in this work are poorly understood, the converted volume-weighted size distributions shown in Figure 4 are only crude representations of the actual ones. For hydrodynamic diameters greater than 100 nm, the DLS- and NTA-originating volume-weighted distributions show a satisfactory agreement, perhaps except those for the BH site where the DLS-determined distribution peaks at a somewhat larger particle size. It is worth noting that since particle volume increases with the cube of particle diameter, the volume-weighted distribution functions from NTA are significantly magnified for large diameters. In some cases, they may seem to dominate the distributions, despite having a low particle count in that diameter range.

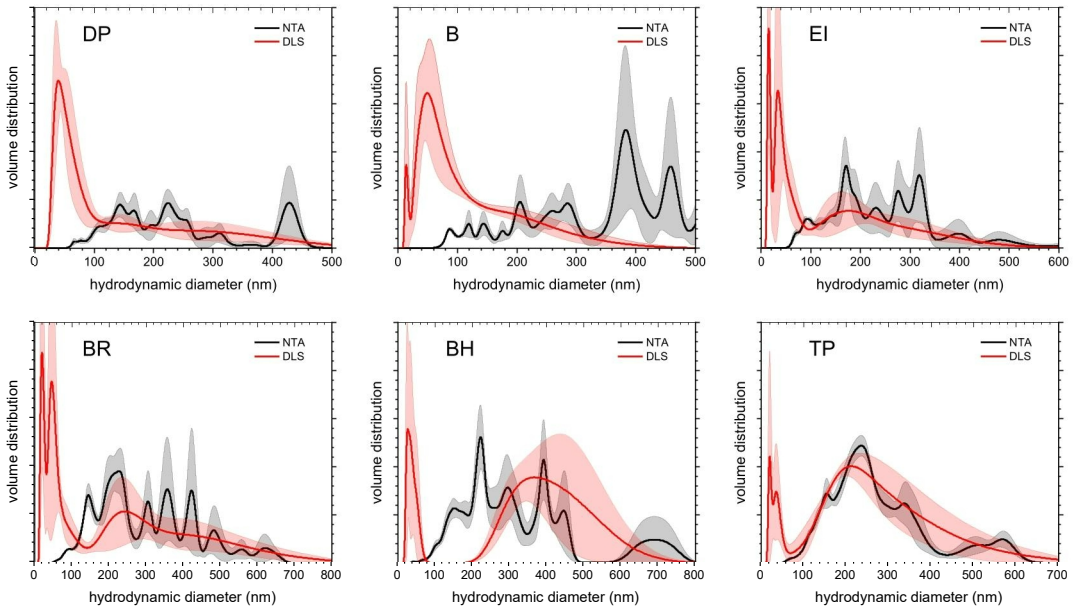

Figure 4. Comparison of volume-weighted hydrodynamic diameter distributions measured by dynamic light scattering (red) and nanoparticle tracking analysis (black). Solid lines indicate average distributions from three (DLS) and five (NTA) measurements. The light red (DLS) and gray (NTA) bands correspond to one standard error interval. Volume-weighted distributions were converted from the native distributions of DLS and NTA, intensity- and number-weighted, respectively.

A notable feature observed in Figure 4 across all six sites is the peak of volume-weighted distributions from DLS at hydrodynamic diameters below 100 nm, while the distribution functions from NTA decrease to zero as the diameter decreases. The presence of small particles, some as small as 10 nm in diameter, is evident in the intensity-weighted distributions in Figure 3. Considering that the scattering cross-section scales for small particles with the sixth power while their volume scales only with the cube of particle diameter, it is understandable that the volume-weighted distributions (Figure 4) peak in the diameter range below 100 nm. Furthermore, this indicates that the majority of particles with diameters smaller than 100 nm, particularly below 50 nm, were not observed or counted in the NTA experiments (Figure 3), resulting in a severely underestimated number concentration.

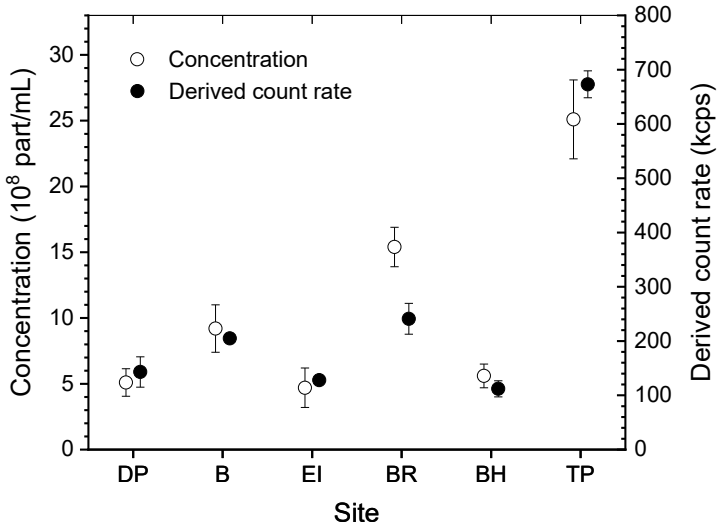

Figure 5. Comparison of number concentrations determined by NTA (open circles) with derived count rates measured by DLS (closed circles). Error bars indicate three standard errors.

Particle number concentrations measured by NTA and derived count rates of the six Group A samples are illustrated in Figure 5. Given the high polydispersity of the Group A samples, it was not expected that DCR values would exhibit proportionality with particle number concentration, C_N. Surprisingly, the DCRs appeared to be as good indicators of particle number concentration, with the proportionality factor of 4125 showing strong agreement with CN for five out of six sites, as evident in Figure 5. Such

good agreement may suggest similarities in the origin, composition, and/or morphology of the particles detected at these sites.

Size and concentration assessment of Group B

Size measurements of Group B proved challenging due to their limited number and lack of dispersion in solution. Attempting to disperse them was deemed impractical as it risked losing a portion of the particles, particularly considering they couldn't reach an optimal concentration for measurement using DLS. An attempt was made to measure the sample without any size separation; essentially, a solution encompassing all particles from Groups A and B was prepared. Nevertheless, the combination of polydispersity, low sample concentration, and the presence of particles possibly larger than 10 µm in a heterogeneous sample contributed to very wide and irreproducible size distributions, as well as a low signal-to-noise ratio. Consequently, the data obtained was deemed unreliable, and including it in the report would be misleading.

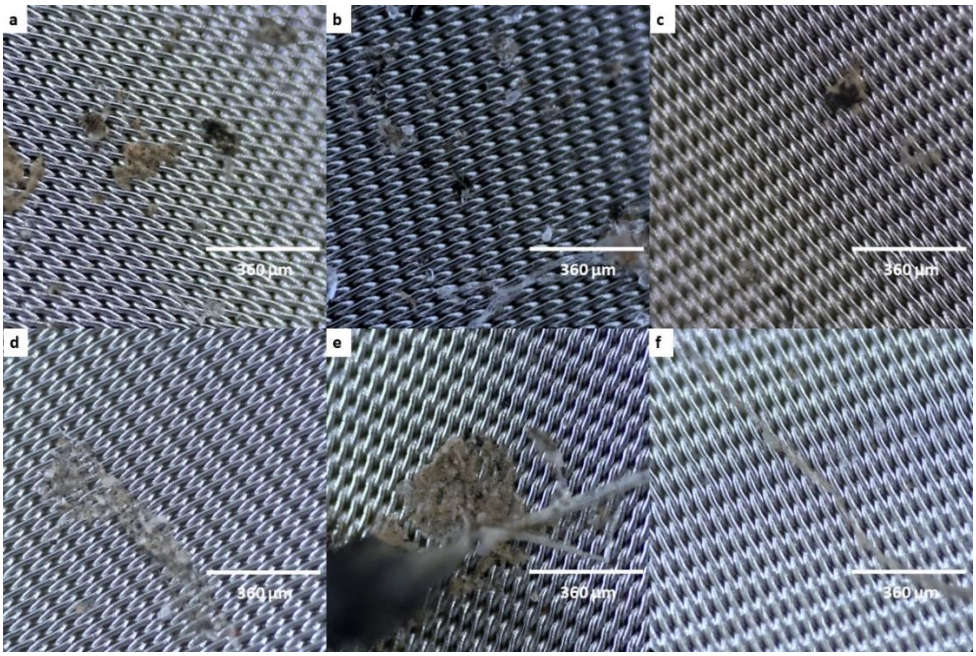

Figure 6. Representative Microscopic images of particles collected on 5 µm stainless steel mesh filters used in vacuum filtration from six sites: Base Hopedale (a), Bevy Road (b), Black Heads (c), Dump Pond (d), Ellen Island (EI), and Trout Pond (TP).

Figure 6 displays microscopic images of particles filtered from 150 mL samples of six sites with 5 µm mesh stainless steel filters. By manually counting the number of particles from six images for each sample, an average number of particles was calculated, and an approximate count of particles per filter (also per site) was determined, listed in Table 1. The filtrates were subsequently filtered through 1 µm PTFE filters and imaged; however, they revealed a minimal quantity of particles, indicating that the size range (between 1 and 5 µm) may not hold significant relevance within the scope of the following experiments. Similar to the findings of low particle concentrations in Group A samples, the particle counts in Group B samples were also low. Among the sites, BR showed the highest particle count, followed by B, EI, DP, BH, and TP, in descending order.

Viability assessment of cells treated with Groups A and B

Several studies have reported the risks associated with anthropogenic nanoparticles such as zinc oxides, carbon nanotubes, cellulose, and nanoplastics.[33-34] Accumulation of these particles has been reported in wildlife such as mammals[35] and birds[36] and is a growing concern, particularly in remote and pristine regions where local human populations are dependent on wildlife for sustenance. These particles have been shown to negatively affect cell viability, cause increased apoptosis, and induce inflammation in in vitro culture systems.[33]

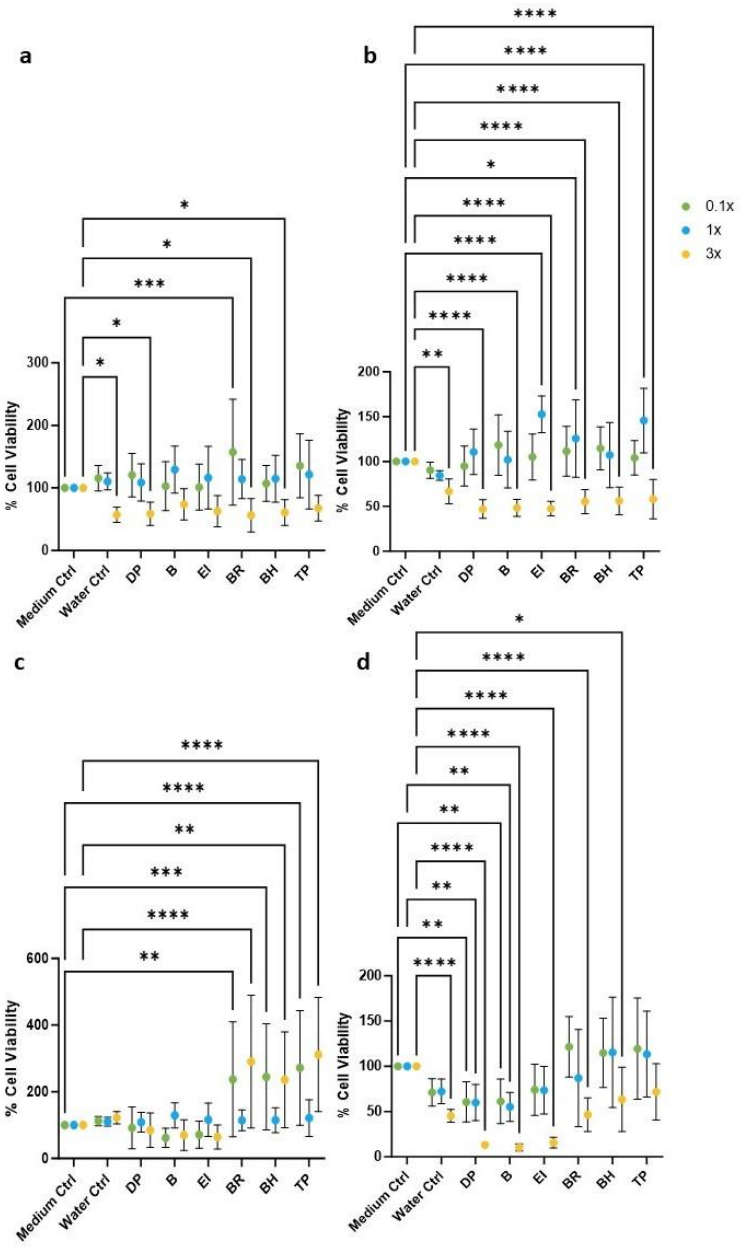

Figure 7. Viability assessment of NB4 (a,b) and NIH3T3 (c, d) cells treated with 0.1x, 1x and 3x of Group A samples in media after 24 h (a, c) and 48 h (b,d). Statistical significance was determined with two-way ANOVA test. $P < 0.05$ was considered significant. *$P < 0.05$; **$P < 0.01$; ***$P < 0.001$; ****$P < 0.0001$. Although comparisons were made between the mean of 6 wells from each group and the control for all data, these are not depicted on the graph unless they demonstrate a statistically significant difference.

To explore the effects of particles in the population of Group A particles, concentrated (10×) particles were dispersed in the treated medium to obtain 0.1, 1, and 3× of Group A (Set 1), respectively, and tested against two controls at two different time points (24 and 48 h) across all six sites with two cell lines, namely NB4 and NIH3T3 (Figure 7). The medium control refers to cells growing in an untreated medium. Water control refers to cells growing in a medium to which water was added, matching the aqueous composition of the treated samples but without any dispersed particles. It was observed that cell viability did not show any significant decrease at treatment with 0.1 and 1× of Group A when compared to the controls.

However, a clear and consistent decrease in cell viability became apparent at the 3× of Group A treatments. Interestingly, this decrease was strongly linked to the water content present in the treatment rather than the nanoparticles themselves. This was indicated by the similar results in the controls with equivalent volume of water as 3× treatments. This dilution of cell culture media may lower the concentration of nutrients such as growth factors and amino acids, which may impair cell metabolism, leading to loss of homeostasis and reduced viability. Previous reports have shown that dilution of one part media with five parts of diluent can reduce cell viability by up to 17%.[37] These findings suggested that the particles may not have a negative impact on cell viability. To confirm this hypothesis, a revised experiment with lower water content was conducted.

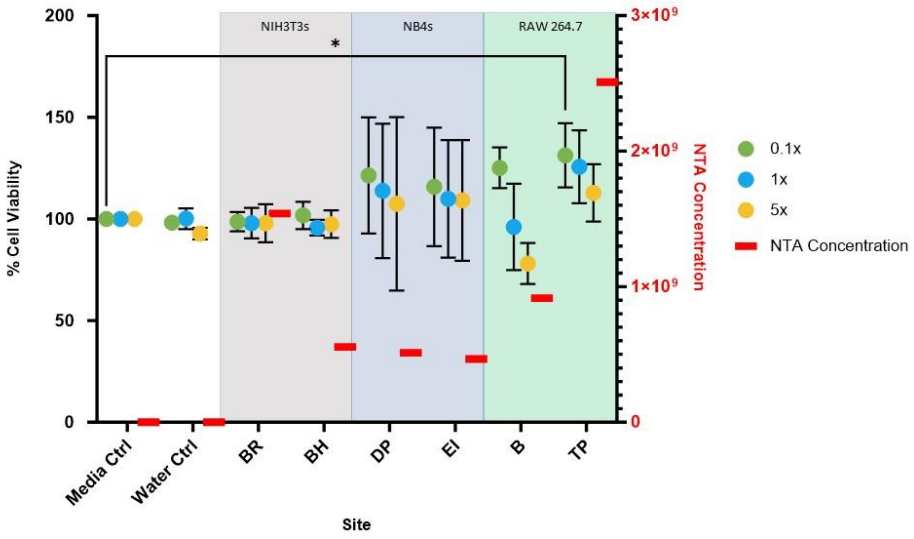

Figure 8. Viability assessment of NIH3T3, NB4, and Raw 264.7 cells after 72 h treatment with 0.1x, 1x, and 5x of Group A in cell culture media. Statistical significance was determined with one-way ANOVA. $P < 0.05$ was considered significant ($*P < 0.05$). The visualization only displays pairwise comparisons that indicate a statistically significant difference among means.

A different set of treatments (Set 2), characterized by lower water content and higher particle concentrations, was tested on three distinct cell lines with samples from two sites each, over 72 h: Raw 264.7 (Sites BR and BH), NB4 (DP and EI), and NIH3T3 (B and TP), as shown in Figure 8. The Group A samples were concentrated by a factor of 100 and added to cell culture media to create suspensions containing 0.1, 1, and 5× concentrations of Group A samples. Unlike the conditions in Figure 7, the revised setup included an additional 24-hour treatment period to allow sufficient time for particle uptake. After 72 h, no significant reduction in cell viability was observed, even at the highest concentration of 5×. The particle concentrations at each site were also presented in Figure 8. Notably, despite higher particle concentrations at sites B, BR, and TP, no significant decrease in cell viability was detected.

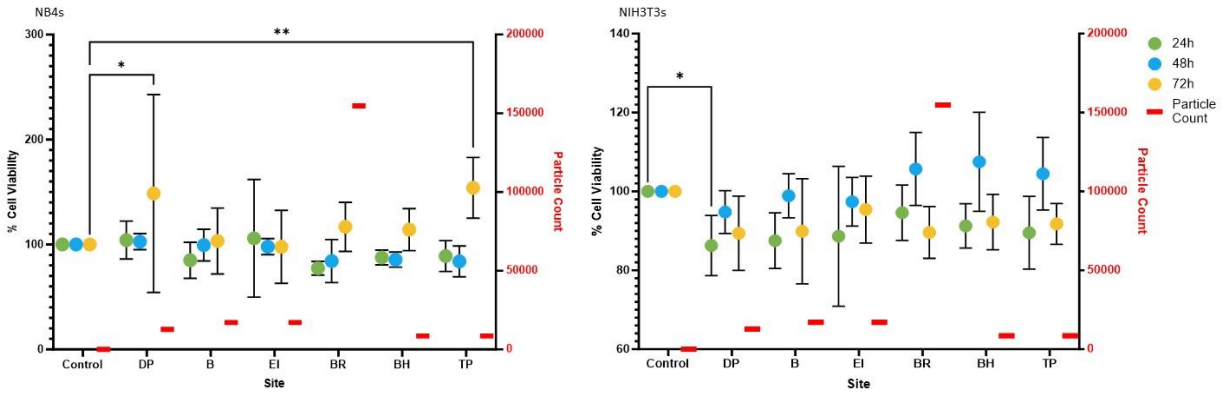

Figure 9. Viability assessment of NIH3T3 and NB4cells after 24h, 48h and 72h treatment Group B. Statistical significance was determined with one-way ANOVA. $P < 0.05$ was considered significant (*$P <$ 0.05). The visualization only displays pairwise comparisons that indicate a statistically significant difference among means.

To explore the effects of particulates in Group B, NB4 and NIH3T3 cells were treated with Group B solution mixed with cell culture media and monitored at intervals of 24, 48, and 72 h. As can be seen from Figure 9, Group B solutions did not perturb cell viability for NB4 cells for any of the time points tested. Similar observations were also made for NIH3T3 cells, where no adverse effect on cell viability was observed for any of the sites or time points tested, except for the 24 h treatment with Group B solution from site DP. Additionally, microscopic observations depicted in Figure 10 present four microscopic images showcasing NIH3T3 cells after 48 h of growth in treated media compared to the control. These images provide a visual representation of cell growth around the particles, highlighting that the particles do not appear detrimental to the cells apart from occupying physical space.

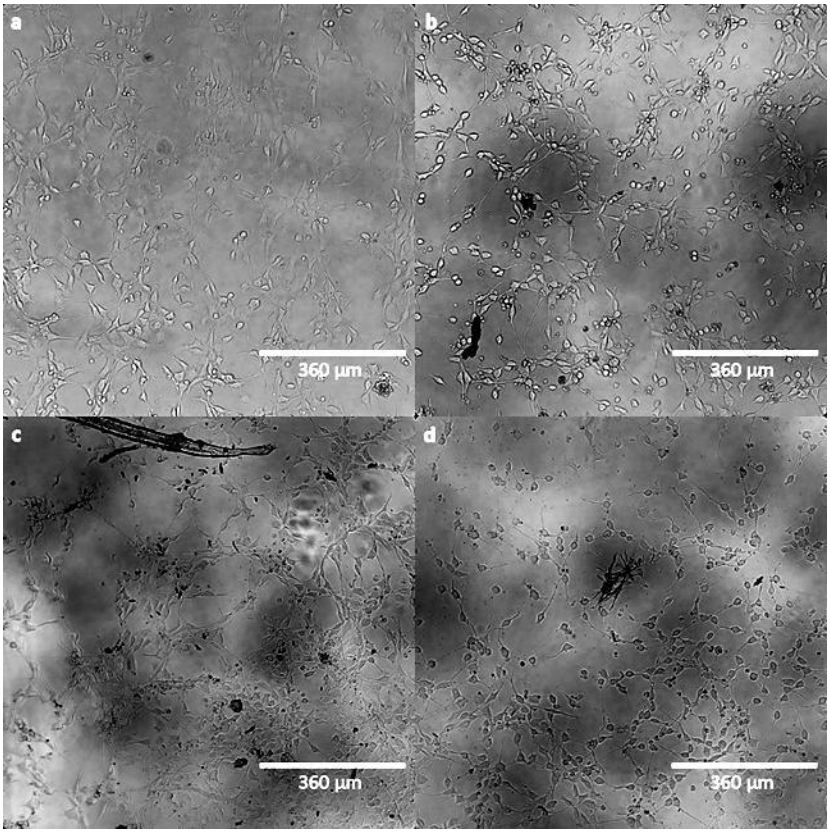

Figure 10. Microscopic images of NIH3T3 cells (48 h) after being treated with Group B (b-d) and the cells in control media(a).

Additionally, an attempt was made to examine the potential correlation between the particle count and percent viability. However, no discernible trend was observed in either Group A (Figure 7) or Group B (Figure SI-4) samples. This absence of correlation suggests that factors beyond particle number—such as particle composition, surface properties, or cell-specific metabolic responses—may influence the observed variability in cellular outcomes. Investigating these factors is critical for improving the interpretability and reproducibility of biological assays that involve heterogeneous environmental particle exposures. Further studies focused on dissecting the mechanisms underlying cell response variability may yield deeper insights into how complex particulate mixtures interact with cellular systems.While this study did not detect a statistically significant correlation between particle count and cell viability, this may be due in part to the limited sample size and number of experimental replicates.

Smaller sample sizes inherently reduce statistical power, making it more challenging to identify subtle but potentially meaningful biological trends. However, these findings highlight an opportunity for future work: increasing the sample size, incorporating additional replicates, and exploring a broader range of particle concentrations. All together this can substantially enhance the sensitivity and robustness of the analysis. Furthermore, employing statistical methods optimized for small-sample datasets could further refine the interpretation of emerging patterns. By building on this foundation, future investigations are well-positioned to more fully characterize the relationship between particle exposure and cell viability, contributing to a deeper understanding of cellular responses under varying experimental conditions.

Inflammation level assessment of cells treated with Group A

In recent years, there has been a growing concern about chronic inflammatory conditions, such as Inflammatory Bowel Disease (IBD), due to exposure to anthropogenic particulates.[33-34] A positive correlation has been reported between the concentration of microplastic particles in feces and the severity of IBD.[34] Similarly, environmental cellulose nanomaterials have been shown to cause acute lung inflammation.[38] While exposure to the particles in Group A did not directly affect cell viability, it may pose a risk of inflammatory conditions. The concentration of TNF-α, a pro-inflammatory cytokine, was measured to evaluate any potential for inflammation. TNF-α, produced by both epithelial cells and immune cells upon exposure to microorganisms and foreign entities, is a robust biomarker of inflammation and is responsible for activating other inflammatory cytokines, such as interleukin-8 and matrix metalloproteinases.[39-41] Results of the inflammation assay, as shown in Table 5, indicated a low extrapolated concentration of TNF-α (all smaller than 4 pg/mL), similar to the control tests (48 h: 3.3 pg/mL; 72 h: 3.6 pg/mL). This indicated that Group A samples, which contain up to 2.5×10^9 (Figure 8, 5× concentrated) smaller than 1 μm particles, did not elicit an inflammatory response in the Raw 264.7 macrophages, suggesting a healthy, viable cell population that is not under stress or damage.[42]

Table 5. The concentration of TNF-α after treatment with Group A.

	Control (Cell) 48 h	Group A 1× (BH) 48 h	Group A 5× (BH) 48 h	Control (Cell) 72 h	Group A 1× (BH) 72 h	Group A 5× (BH) 72 h
TNF-α (pg/mL)	3.3	3.1	3.1	3.6	3.2	3.6

*TNF-α level was measured at 2.9 pg/mL after 72 h of treatment with 10% MilliQ in the media.

Considering the above analyses, the particles in Group A collected from the Hopedale region did not elicit any negative cellular response, including inflammation, even after a fivefold concentration with a 72 h treatment. However, realistic long-term or chronic exposures to these APs may still pose a risk to human or animal health. Thus, longer-duration treatments in animal and in vitro models may be warranted.

Conclusion

This study provides new insights into the dynamics of small particles within snow samples collected from six distinct sites in the Hopedale region of Nunatsiavut, Canada. Analysis of eighteen snow samples revealed consistent particle sizes across locations, but notable variations in concentration. Trout Ponds exhibited the highest particle concentrations, followed by Berry Road, suggesting the influence of localized environmental factors on particle accumulation.

Our findings emphasize the importance of examining particle sources in environmental samples when evaluating their potential biological effects. Using cell models representing fibroblasts (NIH3T3), macrophages (RAW 264.7), and blood-derived cells (NB4), we assessed particle-induced changes in cell viability. Larger particles may reflect the aggregation or settling of smaller counterparts, but their relatively low abundance appeared to exert limited biological impact. Notably, no direct correlation was observed between particle concentration and cellular response, suggesting that complex physicochemical and biological factors modulate cell-particle interactions.

Particles smaller than 100 nm, especially those below 50 nm, were likely underrepresented due to instrumental limitations in NTA. However, these smaller particles still contributed to the cellular responses observed, highlighting the need for improved detection methods and more comprehensive particle characterization in future studies to better inform dose–response assessments.

Through the use of analytical tools such as DLS and NTA, this study enhances our understanding of the interactions between environmental particulates and cellular systems. These insights contribute to a broader understanding of how snowborne particles may influence biological systems in northern environments.

Looking ahead, continued research is essential to uncover the mechanisms governing particle–cell interactions and to inform strategies for minimizing potential health risks. A nuanced understanding of snow particle dynamics is particularly relevant for protecting environmental and human health in snow-rich regions such as Hopedale.

In light of the absence of any observed toxic effects on cellular viability, it could be argued that pinpointing the specific type of particles might not be imperative. Since the primary concern revolves around the potential harm to cellular functions, the identification of particle types may not significantly alter the study's outcome. This stance is supported by the fact that regardless of the particle composition, their presence did not correlate with detrimental effects on cellular viability. Thus, prioritizing the understanding of how these particles interact with biological systems and their subsequent impact on cellular responses could be deemed more pertinent than focusing solely on particle identification.

Acknowledgments

We thank the Nunatsiavut Government Land and Natural Resources team and Jess Melvin for supporting the project logistics and sample stewardship.

Competing interest statement

The authors declare that there are no competing interests.

Author contribution statement

Z.M. and S.Z. were responsible for conceptualization; E.T. was responsible for site selection and sample collection; E.T., L.P., and M.L were responsible for collection protocol methods; Z.M., S.S., and S.Z. were responsible for methodology; Z.M. was responsible for formal analysis; Z.M. S.S. and Z.J. were responsible for investigation; Z.M., Z.J. and S.Z. were responsible for data curation; Z.M., Z.J., and S.S. was responsible for visualization; Z.M. S.S., Z.J. and S.Z. were responsible for writing the original draft; S.Z. was responsible for resources, supervision and funding acquisition, M.L. and S.Z were responsible for project administration; All were responsible for reviewing and editing.

Funding statement

The authors appreciate the Arctic and Northern Challenge Program at the National Research Council Canada (NRC), the Advancing a Circular Plastics Economy for Canada Program from the Government of Canada and the Canada-Inuit Nunangat-United Kingdom Arctic Research (CINUK) Program, and the Nunatsiavut Government for financial support.

Data availability statement

Data generated or analyzed during this study are available from the corresponding author upon reasonable request. The Nunatsiavut Government owns sample data.

References

1. Brandt, J. P.; Flannigan, M. D.; Maynard, D. G.; Thompson, I. D.; Volney, W. J. A. An introduction to Canada's boreal zone: ecosystem processes, health, sustainability, and environmental issues. *Environmental Reviews*, **2013,** *21* (4), 207-226.
2. Townhill, B. L.; Reppas-Chrysovitsinos, E.; Sühring, R.; Halsall, C. J.; Mengo, E.; Sanders, T.; Dähnke, K.; Crabeck, O.; Kaiser, J.; Birchenough, S. N. R. Pollution in the Arctic Ocean: An overview of multiple pressures and implications for ecosystem services. *Ambio*, **2022,** *51* (2), 471-483.
3. Huntington, H. P.; Danielson, S. L.; Wiese, F. K.; Baker, M.; Boveng, P.; Citta, J. J.; De Robertis, A.; Dickson, D. M. S.; Farley, E.; George, J. C.; et al. Evidence suggests potential transformation of the Pacific Arctic ecosystem is underway. *Nature Climate Change*, **2020,** *10* (4), 342-348.
4. Wassmann, P.; Duarte, C. M.; Agustí, S.; Sejr, M. K. Footprints of climate change in the Arctic marine ecosystem. *Global Change Biology*, **2011,** *17* (2), 1235-1249.
5. Dauginis, A. L. A.; Brown, L. C. Sea ice and snow phenology in the Canadian Arctic Archipelago from 1997 to 2018. *Arctic Science*, **2021,** *7* (1), 182-207.
6. Tank, S. E.; Manizza, M.; Holmes, R. M.; McClelland, J. W.; Peterson, B. J. The Processing and Impact of Dissolved Riverine Nitrogen in the Arctic Ocean. *Estuaries and Coasts*, **2012,** *35* (2), 401-415.
7. Adams, J. K.; Dean, B. Y.; Athey, S. N.; Jantunen, L. M.; Bernstein, S.; Stern, G.; Diamond, M. L.; Finkelstein, S. A. Anthropogenic particles (including microfibers and microplastics) in marine sediments of the Canadian Arctic. *Science of The Total Environment*, **2021,** *784*, 147155.
8. Tirelli, V.; Suaria, G.; Lusher, A. L. Microplastics in Polar Samples. In *Handbook of Microplastics in the Environment*, Rocha-Santos, T.; Costa, M. F.; Mouneyrac, C., Eds. Springer International Publishing: Cham, 2022; pp 281-322.
9. Bianco, A.; Sordello, F.; Ehn, M.; Vione, D.; Passananti, M. Degradation of nanoplastics in the environment: Reactivity and impact on atmospheric and surface waters. *Science of The Total Environment*, **2020,** *742*, 140413.
10. Bond, T.; Ferrandiz-Mas, V.; Felipe-Sotelo, M.; Van Sebille, E. The occurrence and degradation of aquatic plastic litter based on polymer physicochemical properties: A review. *Critical Reviews in Environmental Science and Technology*, **2018,** *48* (7-9), 685-722.
11. Dris, R.; Gasperi, J.; Saad, M.; Mirande, C.; Tassin, B. Synthetic fibers in atmospheric fallout: A source of microplastics in the environment? *Marine Pollution Bulletin*, **2016,** *104* (1-2), 290-293.
12. Materić, D.; Kjær, H. A.; Vallelonga, P.; Tison, J.-L.; Röckmann, T.; Holzinger, R. Nanoplastics measurements in Northern and Southern polar ice. *Environmental Research*, **2022,** *208*, 112741.
13. Boutron, C. F.; Candelone, J.-P.; Hong, S. Past and recent changes in the large-scale tropospheric cycles of lead and other heavy metals as documented in Antarctic and Greenland snow and ice: A review. *Geochimica et Cosmochimica Acta*, **1994,** *58* (15), 3217-3225.
14. Steffen, A.; Bottenheim, J.; Cole, A.; Ebinghaus, R.; Lawson, G.; Leaitch, W. R. Atmospheric mercury speciation and mercury in snow over time at Alert, Canada. *Atmospheric Chemistry and Physics*, **2014,** *14* (5), 2219-2231.

15. Halsall, C. J. Investigating the occurrence of persistent organic pollutants (POPs) in the arctic: their atmospheric behaviour and interaction with the seasonal snow pack. *Environmental Pollution*, **2004,** *128* (1-2), 163-175.
16. Doherty, S. J.; Dang, C.; Hegg, D. A.; Zhang, R.; Warren, S. G. Black carbon and other light-absorbing particles in snow of central North America. *Journal of Geophysical Research: Atmospheres*, **2014,** *119* (22), 12807-12831.
17. Doherty, S. J.; Warren, S. G.; Grenfell, T. C.; Clarke, A. D.; Brandt, R. E. Light-absorbing impurities in Arctic snow. *Atmospheric Chemistry and Physics*, **2010,** *10* (23), 11647-11680.
18. Macdonald, R. W.; Barrie, L. A.; Bidleman, T. F.; Diamond, M. L.; Gregor, D. J.; Semkin, R. G.; Strachan, W. M. J.; Li, Y. F.; Wania, F.; Alaee, M.; et al. Contaminants in the Canadian Arctic: 5 years of progress in understanding sources, occurrence and pathways. *Science of The Total Environment*, **2000,** *254* (2-3), 93-234.
19. *AMAP Assessment 2021: Human Health in the Arctic*. Arctic Monitoring and Assessment Programme (AMAP): Tromsø, Norway, 2021.
20. *Effects of Plastic Pollution on Arctic Animals. Summary for Policy-makers*. Arctic Monitoring and Assessment Programme (AMAP): Tromsø, Norway, 2025.
21. Yee, M. S.; Hii, L. W.; Looi, C. K.; Lim, W. M.; Wong, S. F.; Kok, Y. Y.; Tan, B. K.; Wong, C. Y.; Leong, C. O. Impact of Microplastics and Nanoplastics on Human Health. *Nanomaterials*, **2021,** *11* (2), 496.
22. Warheit, D. B.; Laurence, B. R.; Reed, K. L.; Roach, D. H.; Reynolds, G. A.; Webb, T. R. Comparative pulmonary toxicity assessment of single-wall carbon nanotubes in rats. *Toxicological Sciences*, **2004,** *77* (1), 117-125.
23. Hildebrandt, L.; Mitrano, D. M.; Zimmermann, T.; Pröfrock, D. A Nanoplastic Sampling and Enrichment Approach by Continuous Flow Centrifugation. *Frontiers in Environmental Science*, **2020,** *8*, 89.
24. Bjarnsholt, T. The role of bacterial biofilms in chronic infections. *APMIS*, **2013,** *121* (s136), 1-58.
25. Saveyn, H.; De Baets, B.; Thas, O.; Hole, P.; Smith, J.; Van Der Meeren, P. Accurate particle size distribution determination by nanoparticle tracking analysis based on 2-D Brownian dynamics simulation. *Journal of Colloid and Interface Science*, **2010,** *352* (2), 593-600.
26. Wright, M. Nanoparticle Tracking Analysis for the Multiparameter Characterization and Counting of Nanoparticle Suspensions. In *Nanoparticles in Biology and Medicine*, Soloviev, M., Ed. Humana Press: Totowa, NJ, 2012; Vol. 906, pp 511-524.
27. Gross, J.; Sayle, S.; Karow, A. R.; Bakowsky, U.; Garidel, P. Nanoparticle tracking analysis of particle size and concentration detection in suspensions of polymer and protein samples: Influence of experimental and data evaluation parameters. *European Journal of Pharmaceutics and Biopharmaceutics*, **2016,** *104*, 30-41.
28. Filipe, V.; Hawe, A.; Jiskoot, W. Critical Evaluation of Nanoparticle Tracking Analysis (NTA) by NanoSight for the Measurement of Nanoparticles and Protein Aggregates. *Pharmaceutical Research*, **2010,** *27* (5), 796-810.
29. Präbst, K.; Engelhardt, H.; Ringgeler, S.; Hübner, H. Basic Colorimetric Proliferation Assays: MTT, WST, and Resazurin. In *Cell Viability Assays*, Gilbert, D. F.; Friedrich, O., Eds. Springer New York: New York, NY, 2017; Vol. 1601, pp 1-17.

30. Chamchoy, K.; Pakotiprapha, D.; Pumirat, P.; Leartsakulpanich, U.; Boonyuen, U. Application of WST-8 based colorimetric NAD(P)H detection for quantitative dehydrogenase assays. *BMC Biochemistry*, **2019,** *20* (1), 4.
31. Alhajj, M.; Zubair, M.; Farhana, A. *Enzyme Linked Immunosorbent Assay*. StatPearls Publishing: Treasure Island (FL), 2023.
32. Arnold, R.; König, B.; Galatti, H.; Werchau, H.; König, W. Cytokine (IL-8, IL-6, TNF-alpha) and soluble TNF receptor-I release from human peripheral blood mononuclear cells after respiratory syncytial virus infection. *Immunology*, **1995,** *85* (3), 364-72.
33. Kumah, E. A.; Fopa, R. D.; Harati, S.; Boadu, P.; Zohoori, F. V.; Pak, T. Human and environmental impacts of nanoparticles: a scoping review of the current literature. *BMC Public Health*, **2023,** *23* (1), 1059.
34. Yan, Z.; Liu, Y.; Zhang, T.; Zhang, F.; Ren, H.; Zhang, Y. Analysis of Microplastics in Human Feces Reveals a Correlation between Fecal Microplastics and Inflammatory Bowel Disease Status. *Environmental Science & Technology*, **2022,** *56* (1), 414-421.
35. Álvarez-Méndez, S. J.; Díaz-Peña, F. J.; Gómez-Escabia, S.; González-Sálamo, J.; Hernández-Borges, J. Tracking anthropogenic microparticles in wildlife of an alpine insular environment. *Journal of Hazardous Materials*, **2024,** *465*, 133291.
36. Wayman, C.; González-Pleiter, M.; Fernández-Piñas, F.; Sorribes, E. L.; Fernández-Valeriano, R.; López-Márquez, I.; González-González, F.; Rosal, R. Accumulation of microplastics in predatory birds near a densely populated urban area. *Science of The Total Environment*, **2024,** *917*, 170604.
37. Chen, A.; Leith, M.; Tu, R.; Tahim, G.; Sudra, A.; Bhargava, S. Effects of diluents on cell culture viability measured by automated cell counter. *PLOS ONE*, **2017,** *12* (3), e0173375.
38. Ede, J. D.; Ong, K. J.; Goergen, M.; Rudie, A.; Pomeroy-Carter, C. A.; Shatkin, J. A. Risk Analysis of Cellulose Nanomaterials by Inhalation: Current State of Science. *Nanomaterials*, **2019,** *9* (3), 337.
39. Delgado, M. E.; Brunner, T. The many faces of tumor necrosis factor signaling in the intestinal epithelium. *Genes & Immunity*, **2019,** *20* (8), 609-626.
40. Sakib, S.; Zou, S. Attenuation of Chronic Inflammation in Intestinal Organoids with Graphene Oxide-Mediated Tumor Necrosis Factor-α_Small Interfering RNA Delivery. *Langmuir*, **2024**, 3402-3413.
41. Zelová, H.; Hošek, J. TNF-α signalling and inflammation: interactions between old acquaintances. *Inflammation Research*, **2013,** *62* (7), 641-651.
42. Zhao, S.; Jiang, J.; Jing, Y.; Liu, W.; Yang, X.; Hou, X.; Gao, L.; Wei, L. The concentration of tumor necrosis factor-α determines its protective or damaging effect on liver injury by regulating Yap activity. *Cell Death & Disease*, **2020,** *11* (1), 70.